# Mid-infrared Quantum Cascade Laser Integrated with Distributed Bragg Reflector

Jun-ichi HASHIMOTO*,  Hiroyuki YOSHINAGA,  Yukihiro TSUJI,  Hiroki MORI,
Makoto MURATA,  and  Yasuhiro IGUCHI

To achieve a high facet reflectivity needed for the threshold current reduction ($I_{th}$) of a quantum cascade laser (QCL), we have developed an InP-based 7-μm Fabry-Perot (FP) QCL integrated with a distributed Bragg reflector (DBR). The DBR consists of semiconductor walls and air gaps which are alternately arranged by periodically etching the epitaxial layers of the air gap regions. The incorporation of a pair of $3\lambda/4$ DBRs increased the facet reflectivity up to 66%, which was more than twice as high as that of a cleaved facet, and reduced $I_{th}$ by 11%. This DBR-integrated FP-QCL succeeded in oscillation at up to 100°C in pulse operation and at up to 15°C in continuous wave operation, which is the first report on the operation of InP-based DBR-integrated QCLs. It also achieved sufficient output for sensing (up to dozens of mW). The DBR is expected to be used as a low-loss reflector suitable for front facet of QCLs.

Keywords: quantum cascade laser, QCL, mid-infrared, gas sensing, low power-consumption

## 1. Introduction

The mid-infrared (MIR) region (e.g., 3-20 μm) has many optical absorption lines attributed to fundamental vibrational resonances of the molecules of major industrial and environmental gases (e.g., $CO_x$, $NO_x$, $SO_x$), and therefore it is called "the molecular fingerprint region."

The optical absorption attributed to fundamental vibrational resonance is several orders of magnitude higher than that attributed to higher-order harmonics in the near infrared (NIR) region. This helps achieve a highly sensitive (ppb – ppt) optical gas sensor.[1]

Recently, quantum cascade lasers (QCLs)[2] have been drawing attention as new light sources in the MIR region. QCLs are semiconductor lasers developed in 1994 that can oscillate in the MIR region. There has been a growing effort to develop QCLs as compact, high-speed, and narrow linewidth MIR light sources.

Gas sensors using QCLs as the light source offer various advantages such as compactness, high-speed, and high-sensitivity due to the characteristics of QCLs noted above. Such sensors are expected to play a key role as measuring instruments in various fields such as measuring of process and exhaust gases at plants, monitoring of environmental gases, medical diagnosis (e.g., breath analysis), and detection of dangerous materials, and the market is expected to expand rapidly.

The core region (light emitting region) of QCLs consists of superlattice structure.*1 In the core region, a function peculiar to the superlattice is utilized for oscillation in MIR-region: in the core region, radiative transition of carriers (electrons) between subbands of the conduction band in the active region, and subsequent carrier transport to the next active region through the mini-bands of the injector regions by tunneling effect makes the MIR oscillation possible, which was difficult to achieve in the conventional semiconductor laser.

The technology has been improved since the first successful QCL oscillation in 1994,[2] leading to CW operation[3]-[6] at room temperature (RT), single-mode operation[7]-[9] by introducing the distributed-feedback (DFB) structure that is required for gas detection, and so on, and now QCLs have already been commercialized.

An outdoor measurement is one of the main potential applications of QCL gas sensors. These sensors must be battery-operated to reduce the size and weight for portability. Considering such battery operation, the overall power-consumption of the sensor must be reduced to about 5 W, so that the power-consumption of the QCL (light source) must be low, typically less than 1 W. However, the power-consumptions of currently available QCLs are still high at several watts, and therefore most of these QCLs cannot be readily used for this application. To reduce the power-consumption of QCLs, the threshold current must be reduced, for which it is effective to increase the reflectivity of the facet.

Table 1 shows the results of comparison of three methods to increase the facet reflectivity. A typical method is to coat the facet with a high-reflective film, such as a multilayer dielectric film or a metallic film. However a very thick film of around several μm is needed for the multilayer dielectric film in the MIR region, resulting in a difficulty in its formation. For this reason, a metallic film, Au film in particular, is usually used as the high-reflective film for the MIR region.[4],[8] As the calculation results in Fig. 1 show, the facet reflectivity increases rapidly with the increase in Au film thickness; a high reflectivity close to 100% can be easily attained. Thus, Au film is suitable as

Table 1. Comparison of methods to increase the facet reflectivity

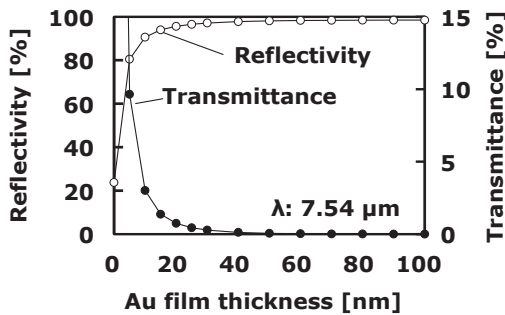| Method | | Multilayer Dielectric Film | Au Film | DBR |
|---|---|---|---|---|
| Facet Reflectivity | > 90% | Unsuitable | Suitable (Especially for Rear Facet) | Unsuitable |
| | 50-80% | | Unsuitable | Suitable (Especially for Front Facet) |

Fig. 1. Au film thickness vs. facet reflectivity and transmittance (calculation)

the total reflection film. It is also easy to form an Au film because a thin Au film of about 100 nm can increase the facet reflectivity sufficiently. Thus, Au film is suited to increasing the reflectivity of the rear facet that requires high reflectivity close to the total reflection (e.g., 90% or higher).

On the other hand, to attain the output power required for a light source of sensing (typically several mW for gas sensing), a moderately high facet reflectivity (50%-80%) is desirable for the front facet so as not to prevent the output light from being reflected excessively by the front facet. However, in the case of Au coating, an ultrathin Au film (10 nm or less) must be used to attain the facet reflectivity in this range (see Fig. 1). This makes it difficult to control the film thickness and quality of the Au film.

In addition, the transmittance decreases rapidly in the MIR region when the film thickness is increased to about 10 nm, as shown in Fig. 1, because the optical absorption of Au is high, so that the output power required for practical use cannot be attained. Thus, it is difficult to apply an Au film as the high-reflective film to the front facet.

To address this issue, we decided to introduce a distributed Bragg reflector (DBR) in place of Au coating, as a means of increasing the facet reflectivity applicable to the front facet. A DBR consists of a high refractive index area and a low refractive index area, which are alternately arranged in a constant period in the direction in which a QCL waveguide extends. The facet reflectivity can be increased in the oscillation wavelength region by integrating the DBR on the facet of a QCL and optimally setting the period of DBR so that Bragg reflection occurs there effectively at the QCL's oscillation wavelength.

The results of comparison between an Au film and DBR are summarized in Table 1. Due to the reasons discussed above, the Au film is effective as a high-reflective (total reflection) film on the rear facet, but it is difficult to apply to the front facet. Meanwhile, a DBR cannot increase the reflectivity to a level equivalent to that of the Au coating (> 90%) due to scattering loss, diffraction loss, etc. but can easily achieve an intermediate reflectivity (e.g., 50%-80%) by controlling the period of DBR and so on. In addition, the absorption loss of a DBR is far smaller than that of an Au coating. Thus, a DBR is suitable for a high-reflective structure on the front facet.

It should also be noted that a DBR can be fabricated together with other QCL structures in the wafer process of fabricating QCL chips, and therefore offers a significant advantage in simplifying the manufacturing process compared to the Au coating in which a wafer must be cleaved to form a chip and an Au film must be formed on its facet.

With laser diodes for optical communication, there have been many reports of increasing the facet reflectivity by introducing a DBR,[10]-[12] but there have been only a few reports with QCLs.[13] As far as we know, there have been no such reports with InP-based QCLs. In this study, we tried to integrate a DBR with a 7 μm-band InP-based FP (Fabry Perot) type QCL to verify its effectiveness. We succeeded in achieving oscillation of an InP-based DBR-QCL for the first time in the world.[14],[15]

## 2. Device Structure

### 2-1 Structure of the main body area

Figure 2 shows the cross-sectional structure of the mesa waveguide in the main body area of the DBR-integrated FP-QCL in the direction in which the waveguide extends.[14],[15] On the InP semiconductor substrate, an n-InP buffer layer, a core region (including 33 laminations of a unit structure consisting of an active region and injection region that were both made by AlInAs/GaInAs superlattices), an n-InP cladding layer, and an n-GaInAs contact layer were successively grown in that order. Then, the semiconductor laminate consisting of the above semiconductor layers was processed into a mesa-stripe, and it was buried by current-blocking layers in the second growth to form a buried-heterostructure (BH) configuration. The current-blocking layer used InP, which is characterized by high thermal conductivity and low optical absorption, to improve the heat dissipation of the device and reduce the internal loss compared to other current confinement structures. The structure is considered to be optimal for reducing the power-consumption of the QCL. Finally, upper and lower electrodes were formed, and thus a device structure was completed.

### 2-2 DBR structure

The DBR structure[14],[15] introduced in this time is also shown in Fig. 2. A DBR structure consisting of pairs of a semiconductor wall (high refractive index area) and a gap (low refractive index area) was integrated on the facet of
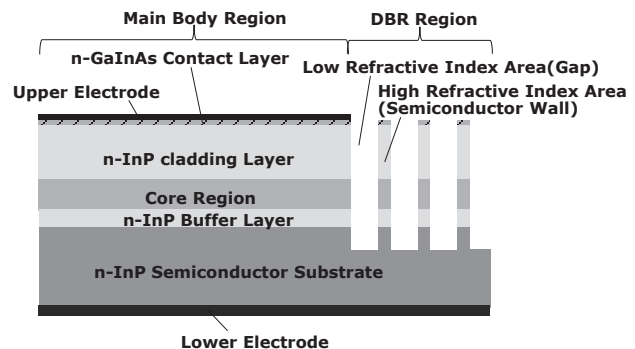


Fig. 2. Device structure of a DBR-integrated FP-QCL

the QCL by periodically dry-etching semiconductor epitaxial layers near the facet of the main body area.

To efficiently increase the reflectivity of a facet using a DBR, the width of $\lambda/(4n)$ or $3\lambda/(4n)$ ($\lambda$: oscillation wavelength in vacuum, n: refractive index of the low refractive index area or high refractive index area) is often used as the width in the direction in which waveguide extends for the high refractive index area and low refractive index area.

The former DBR was named the $\lambda/4$ structure, and the latter DBR was named the $3\lambda/4$ structure. Two-dimensional electromagnetic field analysis software was used to calculate the wavelength dependence of reflectivity of the DBR-integrated facet when the respective DBR structures consisted of one or two pairs.

Note that the widths of the high refractive index area (semiconductor wall) and low refractive index area (gap) of respective DBRs were fixed to values corresponding to $\lambda$ = 7.54 μm in this calculations (see Table 2). As shown in Fig. 3, the $\lambda/4$ structure is superior in terms of increasing the facet reflectivity and reducing the wavelength dependence of the facet reflectivity. However, this structure has a disadvantage in that fabrication in the normal process becomes difficult due to the ultra-thin semiconductor wall width of sub-μm order (see Table 2). Table 3 summarizes the advantages and disadvantages of both DBR structures. In this study, the $3\lambda/4$ structure (a DBR which is easy to fabricate) was used for the first fabrication of the DBR-integrated QCL to put top priority on achieving the successful operation of the QCL.

Table 2. DBR structures used for calculation (for λ=7.54 μm)

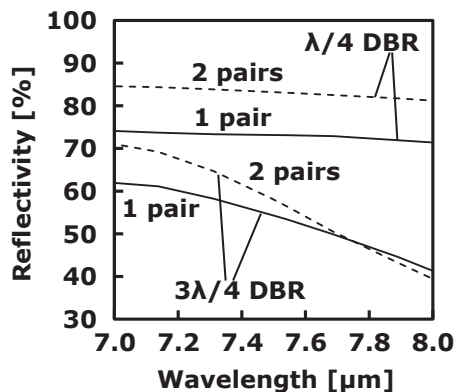| DBR Structure | $\lambda/4$ | $3\lambda/4$ |
|---|---|---|
| Width of High Refractive Index Area (μm) | 0.6 | 1.8 |
| Width of Low Refractive Index Area (μm) | 1.9 | 5.7 |



Fig. 3. DBR facet reflectivity dependence on Wavelength (calculation)

Table 3. Comparison of DBR structures

| DBR structure | $\lambda/4$ | $3\lambda/4$ |
|---|---|---|
| Reflectivity | High | Middle |
| Reflectivity dependence on λ | Small | Large |
| Fabrication | Difficult | Easy |

## 3. Fabrication Process

This section explains the process used to fabricate the device.[14],[15] Organometallic vapor phase epitaxy (OMVPE) was used for crystal growth. In the first growth, the respective semiconductor layers discussed above (which make up the mesa waveguide) were successively grown on an n-InP substrate. Next, the epitaxial layers were etched to the core region or deeper except for the center region of the device to form a mesa waveguide of 10 μm in width. Subsequently, the InP current blocking layer was grown to bury the mesa-side walls and form the BH structure.

The facet region on one side was then periodically etched with the width of $3\lambda/(4n)$ discussed above using photolithography and dry-etching. As a result, the DBR structure consisting of one or two pairs of semiconductor wall and gap was integrated. Finally, electrodes were formed on the top and bottom surfaces. A cleaved (CL) or etched (ET) facet was used on the other side. The rear facet was coated with Au to provide a high-reflective (HR) film as necessary.

Figure 4 shows the DBR structure (two pairs of $3\lambda/4$ structure) that we fabricated. A semiconductor wall in the high refractive index area is etched with high aspect ratio ($> 4$) and high perpendicularity to the substrate. The roughness of the etched surface is about 100 nm or less, which seemed sufficiently flat for the 7 μm-band oscillation wavelength.
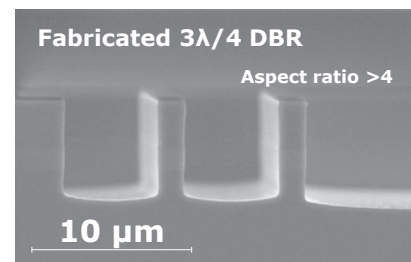


Fig. 4. Scanning electron microscope image of cross-section of DBR structure

## 4. Device Characteristics

### 4-1 Facet reflectivity characteristics of the DBR

First, we evaluated the reflectivity of our fabricated DBR facet as follows.[14],[15] Three types of QCL were formed on the same InP substrate for the evaluation.

(1) QCL1: CL facet for both facets (CL/CL)
(2) QCL2: CL facet for the front facet, and DBR (consisting of one pair of $3\lambda/4$ structure) integrated facet for the rear facet (CL/DBR)
(3) QCL3: CL facet for the front facet, and ET facet (formed under the same dry-etching condition as that of DBR) for the rear facet (CL/ET)

These QCLs have the same BH structure as discussed above. Their device structures are identical except for the facet structure. Regarding QCL1 to QCL3 above, we measured the dependence of threshold current density ($J_{th}$)

on the reciprocal (1/L) of the cavity length (L) at RT and under the pulse condition. The results are shown in Fig. 5. Note that the straight lines in this figure represent linear approximations of measurement data of respective QCLs based on the least squares method.

Here, the relational expression below is valid between the QCL's cavity length (L) and threshold current density $(J_{th})$.[16]

$$J_{th} = \frac{\alpha_w}{\Gamma g} - \frac{\ln(R_f R_r)}{2\Gamma g L}$$

($\alpha_W$: internal loss, $\Gamma$: optical confinement coefficient in the core region, g: optical gain, $R_f$: reflectivity of the front facet, $R_r$: reflectivity of the rear facet).
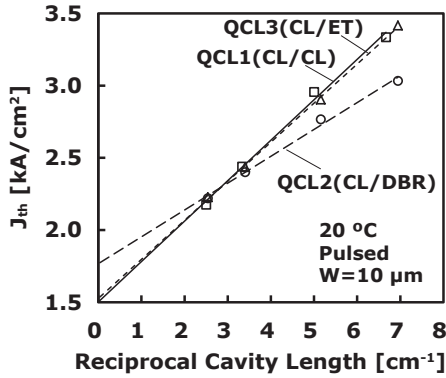


Fig. 5. Dependence of the threshold current density on cavity length

Consequently, first for QCL1, $\Gamma g$ and $\alpha_W$ can be calculated from the inclination and y intercept of the straight line of QCL1, respectively, by assuming the reflectivity of the CL facet applied to $R_f$ and $R_r$ to be 28% and based on the expression above. Then for QCL2, $\Gamma g$ can be assumed to be the same value as that of QCL1 because they have the same main body structure, and $R_f$ can be assumed to be the value for CL facet (28%) mentioned above. Based on these assumptions, $R_r$ (i.e., reflectivity of the DBR facet) and $\alpha_W$ of QCL2 can be calculated from the inclination and y intercept of the approximate straight line of QCL2, respectively. Also for QCL3, $\alpha_W$ and the reflectivity of the ET facet ($R_f$) can be calculated similarly.

Table 4 summarizes the results of rear facet reflectivity ($R_r$) and internal loss ($\alpha_W$) of respective QCLs that were calculated as explained above. For QCL3, the etched (ET) facet and the cleaved (CL) facet have equivalent reflectivities. This result and the observation result in Fig. 4 lead to the conclusion that the etched facet made by the dry-etching used in this study has perpendicularity and flatness equivalent to those of the cleaved facet.

Table 4. $R_r$ and $\alpha_W$ comparison among fabricated QCLs

| QCL | Rear Facet | $R_r$ (%) | $\alpha_W$ (cm$^{-1}$) |
|---|---|---|---|
| QCL1 | CL | 28 (Assumption) | 6.8 |
| QCL2 | DBR | 66 | 8.0 |
| QCL3 | ET | 31 | 6.9 |

For QCL2, the reflectivity of the DBR facet was 66%, which was more than double that of the CL facet. As expected, the results demonstrated that the DBR increases the reflectivity of the QCL facet effectively. Due to the etched surface of the semiconductor wall of DBR with excellent perpendicularity and flatness, Bragg-reelection took place effectively in the DBR region, leading to such high reflectivity.

There is a significant difference between the measured value of facet reflectivity (66%) and calculation result in Fig. 3 (55%) in the case of the DBR using one pair of 3λ/4 structures. Presumably, this difference is attributed to the structural differences between the calculation model and actual DBR (e.g., grating period, etching depth) and errors of optical constants (e.g., refractive index) used in the above calculation. We will correct these parameters to increase the accuracy of the facet reflectivity calculation.

The comparison between QCL1 and QCL3 did not show an increase in the internal loss ($\alpha_W$) even in the case of an etched facet, which suggests that the facet etching was performed with no additional loss. Meanwhile, QCL2 showed an increase in $\alpha_W$ by about 1 cm$^{-1}$. We suppose that this is caused by increased losses attributed to scattering, diffraction, etc. in the DBR structure.

## 4-2 Oscillation characteristics of the DBR- integrated QCL

Now that we verified that the DBR integration significantly increased the reflectivity of the facet based on the above evaluations, we evaluated the oscillation characteristics of the DBR-integrated QCL in the next step.[14],[15] Figure 6 shows the result of comparison of current density-output power characteristics between the above QCL1 and QCL2 chips (cavity length [L]: 2 mm, mesa width [W]: 10 μm) at 20°C under the pulse condition.

$J_{th}$ of QCL2 decreased by 11% compared to QCL1 (2.7 → 2.4 kA/cm$^2$), while the slope efficiency of QCL2 increased by 44% compared to QCL1 (0.16 → 0.23 W/A). This shows the characteristics improvements derived from adding the DBR to the rear facet to increase the facet reflectivity.

Next, we fabricated a DBR/HR QCL chip (L: 2 mm, W: 10 μm) in which in addition to the integration of the above DBR having one pair of 3λ/4 structure (estimated
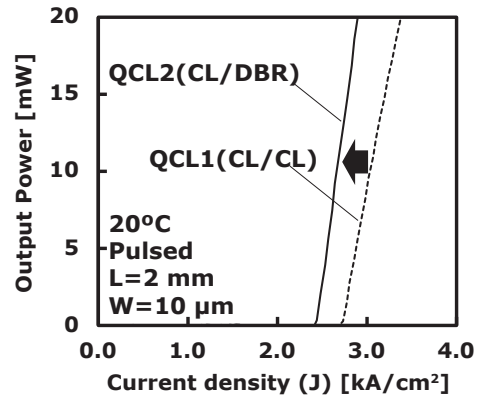


Fig. 6. Change of current density –output power characteristic by DBR introduction

reflectivity: 66%) on the front facet, high-reflective (HR) Au coating (estimated reflectivity: ~ 100%) was performed on the rear facet to further reduce the threshold current ($I_{th}$). We measured the temperature dependence of the current – output power characteristics of the DBR/HR QCL chip in the pulse and CW operations. The obtained characteristics are shown in Figs. 7 and 8. As shown in Fig. 7, the QCL oscillated up to 100°C (measurement limit) in pulse operation. The output power of up to 40 mW (measurement limit) was attained up to 40°C. The $I_{th}$ ($J_{th}$) at 20°C and characteristic temperature ($T_0$) between -40°C and 60°C were 405 mA (2.025 kA/cm$^2$) and 126 K, respectively. As an output power exceeding 40 mW was attained as discussed above, we verified that the DBR structure functions as a low-loss and high-reflective facet structure in the MIR region, as initially expected.
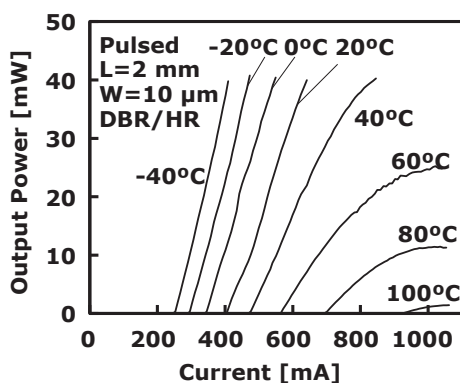
ence of maximum oscillation temperature between in the CW and in the pulse operations, the temperature rise in the device needs to be suppressed during CW operation to enable operation at higher temperatures. For this purpose, we will introduce several improvements such as improving the heat dissipation performance of the device (e.g., reduction in the mesa width, epidown mounting scheme) and further reducing the threshold current by optimizing the device structure (e.g., core structure, doping profile).

Figure 9 shows the oscillation spectrum of the DBR/HR QCL in CW operation at 10°C. Two-mode oscillation was attained with the main peak at the 7.46 μm band, which was almost coincident with the designed value. However, as single mode operation is required for application to gas sensing, we will try to apply the DBR structure to DFB-QCL in the future.



Fig. 7. Current – output power characteristics of DBR-QCL (Pulse)



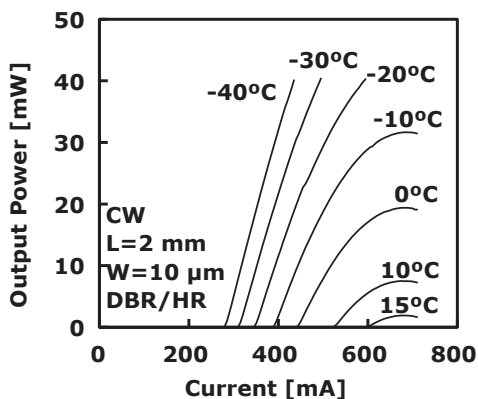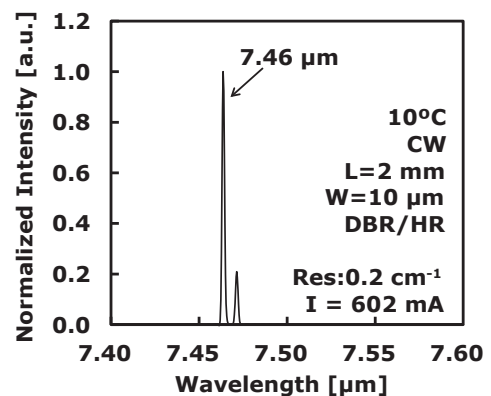Fig. 9. Lasing spectrum of DBR-QCL



Fig. 8. Current – output power characteristics of DBR-QCL (CW)

As shown in Fig. 8, we succeeded in achieving oscillation at RT (up to 15°C) in CW operation. $I_{th}$ ($J_{th}$) at 15°C was 600 mA (3 kA/cm$^2$), and the output power (about 1.9 mW) at 15°C was found to be usable for gas detection. As far as we know, this is the world's first report on the operation of InP-based DBR-QCL.

As discussed above, the maximum temperature for CW operation was 15°C. Operation at higher temperatures should be attained for practical use. Considering the differ-

## 5. Conclusion

In this study, we used the DBR structure as a new method to increase the facet reflectivity in order to reduce the threshold current and thus reduce the power-consumption. We fabricated a 7 μm-band FP-QCL with the DBR structure integrated into the facet. The DBR had a periodical structure consisting of a semiconductor wall (high refractive index area) and a gap (low refractive index area). The DBR with one pair of 3λ/4 structure attained the facet reflectivity of 66%, which is more than double that of a cleaved facet. We thus demonstrated that the DBR effectively increases the reflectivity of the QCL facet.

We then fabricated a QCL chip in which the above DBR was integrated into the front facet, while the rear facet was coated with Au to increase the facet reflectivity. The QCL chip succeeded in oscillation up to 100°C in pulse operation and up to 15°C in CW operation. Thus, we successfully achieved operation of an InP-based DBR-QCL for the first time. The QCL attained an optical output power between several mW and several tense of mW required for sensing such as gas detection. Based on this result, as initially expected, we demonstrated that the DBR can be used on the front facet as a low-loss and high-reflective structure.

We attained the facet reflectivity of 66% by using a $3\lambda/4$ structure as mentioned. However, the facet reflectivity can be changed to an arbitrary value (e.g., 50-80%) by changing the DBR period, duty ratio, and a pair number of high refractive index area and low refractive index area, etc. DBRs are considered to be useful in practical applications for controlling the facet reflectivity in order to obtain optimal QCL characteristics depending on the needs.

In future works, we will try to optimize the device structure and improve the mounting method to enable CW operation at higher temperatures. We will also develop a DFB-QCL with a DBR integrated to apply it to gas sensing that requires single mode operation.

### Technical Term

∗1 Superlattice: A superlattice consists of two types of ultrathin (thickness: several nm or less) semiconductor layers which are laminated alternately (dozens to hundreds of layers). In the structure, many subband levels are formed in the conduction band. A QCL is a semiconductor laser that oscillates by taking advantage of radiative transition between the subbands.

### References

(1) Mid-Infrared Lasers Market Review and Forecast 2014, Strategies Unlimited (2014)

(2) J. Faist, F. Capasso, D. L. Sivco, C. Sirtori, A. L. Hutchinson, A. Y. Cho, "Quantum Cascade Laser," Science, vol. 264, No. 5158, pp. 553-556 (1994)

(3) M. Beck, D. Hofstetter, T. Aellen, J. Faist, U. Oesterle, M. Ilegems, E. Gini, H. Melchior, "Continuous Wave Operation of a Mid-Infrared Semiconductor Laser at Room Temperature," Science, vol. 295, No. 5553, pp. 301-305 (2002)

(4) J. S. Yu, S. Slivken, A. Evans, L. Doris and M. Razeghi, "High-power continuous-wave operation of a 6 μm quantum-cascade laser at room temperature," Appl. Phys. Lett., vol. 83, No. 13, pp. 2503-2505 (2003)

(5) M. Troccoli, S. Corzine, D. Bour, J. Zhu, O. Assayag, L. Diehl, B. G. Lee, G. Höfler and F. Capasso, "Room temperature continuous-wave operation of quantum-cascade lasers grown by metal organic vapor phase epitaxy," Electron. Lett., vol. 41, No. 19, pp. 1059-1060 (2005)

(6) K. Fujita, S. Furuta, A. Sugiyama, T. Ochiai, T. Edamura, N. Akikusa, M. Yamanishi, and H. Kan, "Room temperature, continuous-wave operation of quantum cascade lasers with single phonon resonance-continuum depopulation structures grown by metal organic vapor-phase epitaxy," Appl. Phys. Lett., vol. 91, 141121 (2007)

(7) J. Faist, C. Gmachl, F. Capasso, C. Sirtori, D. L. Sivco, J. N. Baillargeon, and A. Y. Cho, "Distributed feedback quantum cascade Lasers," Appl. Phys. Lett., vol. 70, pp. 2670-2672 (1997)

(8) J. S. Yu, S. Slivken, S. R. Darvish, A. Evans, B. Gokden, and M. Razeghi, "High-power, room-temperature, and continuous-wave operation of distributed-feedback quantum-cascade lasers at λ~4.8 μm," Appl. Phys. Lett., vol. 87, 041104 (2005)

(9) T. Edamura, N. Akikusa, A. Sugiyama, T. Ochiai, M. Yamanishi, K. Uehara, and H. Kan, "Single-mode distributed-feedback quantum cascade laser for high sensitivity gas spectroscopy," IEICE Technical Report, vol. 105, LQE2005-119, pp. 29-32 (2005)

(10) T. Baba, M. Hamasaki, N. Watanabe, P. Kaewplung, A. Matsutani, T. Mukaihara, F. Koyama, and K. Iga, "A Novel Short-Cavity Laser with Deep-Grating Distributed Bragg Reflectors," Jpn. J. Appl. Phys. Vol. 35, Part 1, No. 2B, pp. 1390-1394 (1996)

(11) M. M. Raj, J. Wiedmann, S. Toyoshima, Y. Saka, K. Ebihara and S. Arai, "High-Reflectivity Semiconductor/Benzocyclobutene Bragg Reflector Mirrors for GaInAsP/InP Lasers," Jpn. J. Appl. Phys. Vol. 40, pp. 2269–2277 (2001)

(12) M. Kamp, J. Hofmann, A. Forchel, and S. Lourdudoss, "Ultrashort InGaAsP/InP lasers with deeply etched Bragg mirrors," Appl. Phys. Lett., vol. 78, No. 26, pp. 4074-4075 (2001)

(13) S. Golka, M. Austerer, C. Pflügl, A. M. Andrews, T. Roch, W. Schrenk, and G. Strasser, "GaAs/AlGaAs quantum cascade lasers with dry etched semiconductor-air Bragg reflectors," J. of Modern Optics vol. 52, No. 16, pp. 2303-2308 (2005)

(14) H. Yoshinaga, J. Hashimoto, H. Mori, Y. Tsuji, M. Murata, M. Ekawa, and T. Katsuyama, "Mid-infrared quantum cascade laser integrated with distributed Bragg reflector," in Proc. SPIE Photonics West, 9755-101 (2016)

(15) J. Hashimoto, H. Yoshinaga H. Mori, Y. Tsuji, M. Shiozaki, M. Murata, M. Ekawa, Y. Iguchi, and T. Katsuyama, "Mid-infrared quantum cascade laser (QCL) integrated with distributed Bragg reflector (DBR)," IEICE Technical Report, vol. 116, LQE2016-17, pp. 41-46 (2016)

(16) C. Sirtori, J. Faist, F. Capasso, D. L. Sivco, A. L. Hutchinson, and A. Y. Cho, "Pulsed and Continuous-Wave Operation of Long Wavelength Infrared (λ = 9.3 μm) Quantum Cascade Lasers," IEEE J. Quantum Electron., vol. 33, No.1, pp.89-93 (1997)

## Contributors The lead author is indicated by an asterisk (∗).

### J. HASHIMOTO∗
• Dr. Eng.
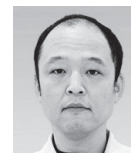Group Manager, Transmission Devices Laboratory

### H. YOSHINAGA
• Assistant Manager, Transmission Devices Laboratory

### Y. TSUJI
• Assistant General Manager, Transmission Devices Laboratory

### H. MORI
• Assistant Manager, Transmission Devices Laboratory

### M. MURATA
• Dr. Sci.
Transmission Devices Laboratory

### Y. IGUCHI
• Dr. Eng.
Department Manager, Transmission Devices Laboratory